Environmental and
Biogeochemical Processes

https://doi.org/10.48130/ebp-0026-0004

Original Research

Open Access

Polymer type, environmental aging, and DOM compositions collectively control DOM fractionation on microplastics

Xiaoxia Zhang[1], Yan Lin[1], Mengting Zhao[1,2], Meiling Zhu[1,3], Tianchi Cao[1*], Thilo Hofmann[4] and Wei Chen[1]

Received: 17 January 2026

Revised: 4 March 2026

Accepted: 18 March 2026

Published online: 30 March 2026

Abstract

Interactions between microplastics (MPs) and dissolved organic matter (DOM) are crucial in controlling MP surface properties, transport, and environmental behavior in aquatic systems. Although DOM adsorption to MPs is well-documented, it remains unclear how polymer type, environmental aging, and DOM composition collectively determine both the extent and selectivity of DOM adsorption on MPs. This study examines DOM adsorption on five common polymers (polyethylene [PE], polypropylene [PP], polyethylene terephthalate [PET], polystyrene [PS], and polyvinyl chloride [PVC]), subjected to controlled UV- and O_3-aging, using Suwannee River fulvic acid (SRFA) and humic acid (SRHA) as representative DOM. For pristine polymers, SRFA exhibited similar distribution coefficients (K_d), whereas SRHA showed pronounced polymer-dependent variability in K_d. Oxidative aging altered DOM adsorption in a strongly polymer- and DOM-specific manner, producing divergent trends in both adsorption capacity and selectivity. The aging pathways (O_3 vs UV) did not monotonically affect DOM fractionation, with O_3-aging inducing a greater increase in the C1 component for PET, and a greater decrease in the C1 component for PS. Fluorescence component analysis and molecular-weight fractionation revealed that aging induced distinct, polymer-specific shifts in the composition and size distribution of DOM retained on MP surfaces. Machine-learning-assisted analysis identified specific surface area and surface carbon speciation (reflecting surface hydrophobicity/hydrophilicity) as the dominant predictors of DOM adsorption behavior. Together, these results demonstrate that DOM fractionation on MPs emerges from the coupled effects of polymer type, weathering-induced surface modification, and DOM characteristics, underscoring the need to account for these factors jointly when predicting MP behavior in real environments.

Keywords: Microplastics, Aging, Dissolved organic matter, Adsorption, Fractionation

Highlights

- SRFA exhibited similar K_d values across pristine MPs, whereas SRHA showed pronounced polymer-dependent variability.
- On PS and PET, SRHA showed higher Kd than SRFA, likely due to SRHA's higher aromaticity.
- On PE and PP, aging boosted hydrophilic, low-MW SRFA retention, consistent with higher microporosity and hydrophilicity.
- Machine learning identifies specific surface area and surface carbon speciation as dominant predictors of K_d for DOM.

* Correspondence: Tianchi Cao (tianchi.cao@nankai.edu.cn)

Full list of author information is available at the end of the article.

https://doi.org/10.48130/ebp-0026-0004

Graphical abstract

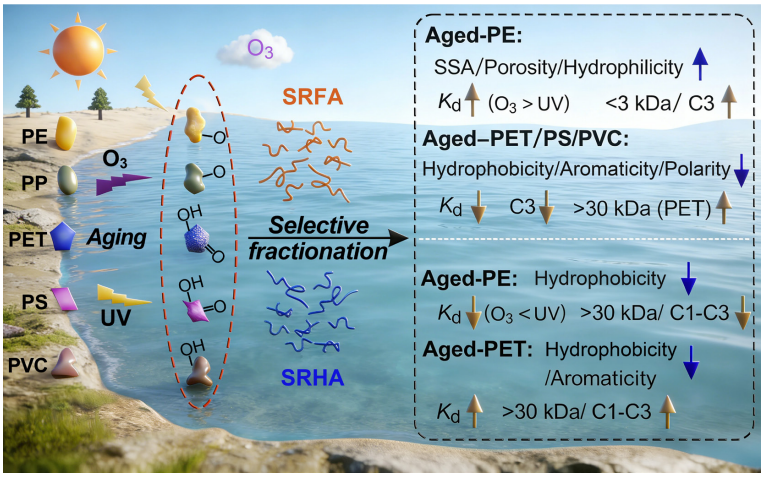

Introduction

Microplastics (MPs) are global emerging pollutants because of their broad distribution and their potential ecological and human-health risks[1–3]. Numerous field surveys have shown that MPs occur in a wide range of environmental matrices, including rivers, lakes, oceans, sediments, and engineered water systems[4,5]. Given their small size and low density, these particles are readily taken up by aquatic organisms across different trophic levels and have been associated with adverse biological responses, such as physical stress and oxidative damage[6–8]. Beyond direct biological effects, MPs serve as 'carriers' for coexisting contaminants (e.g., hydrophobic organic compounds and heavy metals) due to their hydrophobic polymeric matrices and the large specific surface area, thereby potentially altering contaminant transport and bioavailability[9]. In natural waters, MPs inevitably interact with dissolved organic matter (DOM), a chemically heterogeneous mixture that is ubiquitous in natural waters[10]. Adsorption of DOM onto MP surfaces forms an interfacial organic coating (often termed an 'eco-corona'), which can alter the physicochemical properties of MPs and consequently influence MP fate, transport, and biological impacts[11–13]. Therefore, elucidating the mechanisms governing MP–DOM interactions is essential for predicting the environmental behavior of MPs.

DOM adsorption onto MPs involves multiple interfacial interactions, such as hydrophobic and aromatic interactions, electrostatic interactions, and hydrogen bonding, with their relative contributions mediated by both polymer properties and DOM composition[14–16]. Hydrophobic interactions contribute substantially to DOM adsorption on polymer surfaces and are particularly important for nonpolar polymers, including polyethylene (PE), and polypropylene (PP)[17]. In addition, aging can introduce oxygen-containing groups on nonpolar polymers, thereby increasing surface hydrophilicity and polarity, and altering polar interactions (such as hydrogen bonding), which can enhance the adsorption capacity of these MPs for humic acid[18]. For aromatic polymers such as polystyrene (PS), phenyl rings are inherent repeat-unit structures and can be present at or near the surface in both pristine and aged particles; accordingly, π–π stacking interactions between aromatic moieties in DOM and phenyl rings of the polymer backbone contribute substantially to DOM adsorption on both pristine and aged PS microplastics[15,19]. Importantly, MP–DOM interactions are also strongly modulated by DOM heterogeneity (e.g., molecular weight, functional-group composition, and aromaticity)[20,21]. Studies have reported that Suwannee River humic acid (SRHA) exhibits substantially stronger adsorption affinity than Suwannee River fulvic acid (SRFA) onto PS microplastics[15]. These findings indicate that understanding MP–DOM interactions requires not only quantifying bulk adsorption, but also resolving the preferential partitioning and molecular fractionation of DOM on MP surfaces.

Despite growing interest in DOM–MP interactions and well-documented bulk adsorption behavior[10,22], selective association of DOM fractions with different polymer surfaces remain a critical knowledge gap. Specifically, because DOM is a multicomponent mixture (e.g., humic-like and fulvic-like substances, carbohydrates, protein-like components, and other low- and high-molecular-weight constituents), how polymer properties (such as hydrophobicity, polarity, and aromaticity) govern preferential adsorption of specific DOM fractions remain poorly constrained. Moreover, environmental aging of MPs, including UV-driven photooxidation (initiated by direct UV absorption and/or photosensitizers/chromophoric species) and ozonation (via direct ozone attack and/or secondary reactive oxygen species)[23–25], can introduce oxidized surface moieties (e.g., carbonyl- and hydroxyl-bearing groups), as well as alter surface morphology, wettability, and surface charge, thereby modifying DOM adsorption behavior[24,26]. However, the extent to which surface alterations induced by aging control fraction-specific DOM adsorption across common polymers has not been well resolved.

In this work, we assess how polymer chemistry and weathering-induced surface modification together shape both the extent and selectivity of DOM adsorption on microplastics. Five representative polymers (PE, PP, PS, polyvinyl chloride [PVC], and polyethylene terephthalate [PET]), spanning a broad range of backbone chemistries and surface properties were subjected to controlled UV and ozone aging to capture key oxidative weathering pathways relevant to aquatic environments. We used SRFA and SRHA from the International Humic Substance Society (IHSS) as well-characterized DOM reference materials to ensure cross-study comparability[27]. Using both DOM standards captures key compositional differences (e.g., aromaticity, molecular-weight distribution, and functional-group density)[27] that are important for evaluating DOM-dependent adsorption and fractionation on MPs. By integrating bulk adsorption measurements with analyses of DOM composition and

molecular-size distribution at the microplastic–water interface, this work addresses how environmental aging alters not only overall DOM affinity, but also the preferential association of distinct DOM fractions across polymers. Specifically, we aim to: (1) resolve polymer- and DOM-specific shifts in adsorption capacity and fractionation induced by aging; and (2) identify the surface physicochemical properties that govern selective DOM partitioning. Together, these results link measurable surface descriptors to DOM adsorption and fractionation behavior, providing mechanistic insight into DOM–microplastic interfacial chemistry and strengthening the basis for predicting DOM-mediated microplastic behavior in real environmental systems.

Materials and methods

Preparation of aged MPs

Polymer powders of PE, PP, PS, PET, and PVC were supplied by Guanbu Electromechanical Technology Inc. (Shanghai, China). Information on the molecular structures of these MPs is provided in Supplementary Table S1. The average particle size of as-purchased (pristine) microplastics was 61.2 ± 26.4 μm (for PE), 131 ± 45.1 μm (for PP), 24.7 ± 7.2 μm (for PET), 108 ± 36 μm (for PS), and 0.764 ± 0.308 μm (for PVC) (Supplementary Table S2). The pristine MPs were treated by ozone or UVA following adapted literature protocols[28–30], and are denoted with the suffixes '-O_3' and '-UV,' respectively. Briefly, for ozone aging, each type of MP was dispersed at 1 g L^{-1} in a 1-L quartz vessel, and O_3 was continuously delivered into the suspension through a ceramic diffuser at a flow rate of 0.10 L min^{-1} for 5 d at room temperature. Ozone was produced from high-purity O_2 (99.99%) using a 3S-A15 generator (Tonglin Technology Co., Beijing, China). For UV aging, suspensions (3.0 g L^{-1}) in 5 mM $NaNO_3$ were placed in 50 mL quartz tubes and irradiated with 365 nm mercury lamps (500 W; Xujiang Electromechanical Plant, Nanjing, China) for 4 d at room temperature. After aging treatments, MPs were collected using 0.22 μm fiber membranes, sequentially rinsed 3 times with deionized water and ethanol, dried at room temperature in the dark, and stored in amber glass vials. The particle size of MPs generally decreased after aging, particularly for polyolefins like PE and PP, due to processes such as embrittlement and fracture. For other polymers, such as PS and PVC, changes in particle size varied (Supplementary Table S2).

Characterization of MPs

Scanning electron microscopy (S-3400N II, Hitachi, Japan) was used to evaluate the morphology and particle size features of pristine and aged MPs. Their pore volume and specific surface area (SSA) were quantified from N_2 adsorption–desorption isotherms collected at 77 K on a Micromeritics ASAP 2460 porosimetry instrument (Norcross, GA, USA). Molecular-weight parameters, including weight-average molecular weight (M_w), number-average molecular weight (M_n), and polydispersity index (PDI = M_w/M_n) were determined using gel permeation chromatography (PL-GPC 120, Agilent, Waldbronn, Germany). X-ray photoelectron spectroscopy (PHI 5000 VersaProbe, Tokyo, Japan) was used to analyze surface elemental composition and carbon functional groups, while Fourier-transform infrared spectroscopy (Bruker Optics Inc., Karlsruhe, Germany) was applied to identify oxidation-related bands (e.g., C=O, O–H). Wettability was assessed via static water contact angles on pressed pellets/films using an OCA-20 goniometer (Dataphysics Instruments GmbH, Germany). Thermal properties were analyzed by differential scanning calorimetry (Netzsch 204 F1 calorimeter, Selb, Phoenix, Germany) under N_2 (50 mL min^{-1}) with a heating ramp from −150 to 200 °C at a rate of 10 °C min^{-1}. Melting enthalpies and glass transition temperatures (where applicable) were obtained from the thermograms, and the relative crystallinity was estimated from the mass-normalized enthalpy of fusion referenced to literature values for a fully crystalline polymer.

Adsorption experiments of DOM on MPs

Batch adsorption experiments were conducted with SRFA (1–30 mg C L^{-1}) and SRHA (1–30 mg C L^{-1}) obtained from IHSS. Microplastics (0.050 g) were added to 20 mL of 4 mM $NaNO_3$ in amber EPA vials, achieving a solid loading of 2.5 g L^{-1}. The solution pH was set to 7.0 ± 0.1 with 0.1 M HNO_3 or NaOH, and checked before and after equilibration. Vials were rotated at 160 rpm and at room temperature for 5 d, a duration confirmed in preliminary tests to achieve apparent equilibrium. Each treatment was conducted in triplicate. After equilibration, suspensions were passed through prewashed 0.22 μm membranes, and dissolved organic carbon (DOC) was determined with a TOC analyzer (Vario TOC, Elementar, Germany). Adsorbed DOM was then calculated from the difference in DOC concentration by mass balance:

$$q_e = (C_0 - C_e)V/m \quad (1)$$

where, C_0 and C_e represent the DOC concentrations (mg C L^{-1}) in the starting and equilibrated solutions, respectively; m refers to the mass of sorbent (i.e., MPs), and V denotes the solution volume (L). Isotherms (Supplementary Fig. S1) were fitted by nonlinear regression to the Freundlich model:

$$q_e = K_F C_e^{1/n} \quad (2)$$

where, K_F represents the Freundlich affinity coefficient, and $1/n$ is a dimensionless constant. Distribution coefficient (K_d) is obtained from q_e/C_e. Note that K_d represents one of the most important parameters describing the apparent distribution or partitioning equilibrium of DOM between the solution and the microplastic surface, serving as an indicator of overall sorption affinity.

Characterization of DOM molecular fractionation

Fluorescence excitation–emission matrix (EEM) combined with PARAFAC analysis was used to characterize fluorescent DOM fractions before and after adsorption onto MPs. EEMs were collected on an F-7100 spectrofluorometer (Hitachi, Japan), with emission collected from 280 to 550 nm at 1 nm resolution and excitation scanned from 220 to 450 nm in 5 nm steps. Excitation and emission slit widths were both fixed at 5 nm, and spectra were acquired at a rate of 12,000 nm min^{-1}. Raw EEM data were processed by blank correction and adjustment for inner-filter effects using absorbance at the corresponding excitation and emission wavelengths. A 290 nm cutoff filter was used to suppress second-order Rayleigh scattering during data collection. PARAFAC decomposition was conducted in MATLAB R2015b with the DOMFluor toolbox[31–33], as detailed in Supplementary Text S1. Model dimensionality was guided by core-consistency and residual diagnostics, and the resulting model was verified using split-half analysis. Relative abundance of each component was represented by its maximum fluorescence intensity. In total, 110 EEMs from eight independent adsorption experiments were analyzed.

Molecular-weight classes of DOM were obtained by membrane-based size separation. Regenerated-cellulose centrifugal units (Millipore Ultra-15; nominal MWCOs 30 and 3 kDa) were thoroughly rinsed with ultrapure water before use. DOM solutions collected before and after adsorption onto MPs were loaded into 30 kDa centrifugal filters and centrifuged (7,369 rpm, 30 min); the permeate was then

https://doi.org/10.48130/ebp-0026-0004

transferred to 3 kDa filters and centrifuged (9,458 rpm, 30 min). The material retained on the 30 and 3 kDa membranes was recovered by back-rinsing with ultrapure water, and these retentates were assigned to the > 30 kDa and 3–30 kDa fractions, respectively. The permeate from the 3 kDa step constituted the < 3 kDa fraction. Fraction masses were quantified by DOC to determine the distribution of DOM among size classes.

Analysis of key factors controlling DOM distribution coefficients using machine learning

The relationship between MP physicochemical descriptors and the DOM distribution coefficient (K_d) was evaluated using an established neural-network–based workflow[34]. The full dataset was divided once into a training subset and a held-out validation subset. Because the original dataset is limited in size (15 MP surface states and 2 DOM types; Supplementary Tables S2–S4), the training split was used to fit a Wasserstein generative adversarial network (WGAN), which generated ~5,000 synthetic samples to expand coverage of the multivariate descriptor space and support model training/generalization, while approximately preserving the joint feature distribution. The augmented training set (original plus WGAN-generated samples) was used for model development, and the untouched validation set was reserved for performance assessment to avoid information leakage. Continuous predictors (e.g., specific surface area, contact angle, O/C by XPS, roughness, and aging indicators) were standardized, and $\log_{10}K_d$ was modeled to stabilize variance. We benchmarked four regressors—random forest, k-Nearest Neighbors, support vector regression, and a multi-layer perceptron—using cross-validation on the training data. Model performance was assessed on the held-out validation set using the coefficient of determination (R^2), root-mean-squared error, and mean absolute error. Model fidelity was further evaluated by comparing measured and predicted K_d values using parity plots and by inspecting residual error distributions (Supplementary Fig. S2), confirming the reliability of the trained models. To identify controlling factors, we computed permutation feature importance on the best-performing model (primary analysis with Random Forest) and examined response shapes using partial-dependence/accumulated-local-effects profiles, providing interpretable estimates of how surface oxidation, hydrophobicity, charge, and roughness influence K_d.

Results and discussion

Physicochemical characteristics of pristine and aged MPs

The pristine PE, PP, PS, and PET generally displayed irregular shapes and smooth surfaces with varying particle sizes, whereas the pristine PVC was uniquely provided as spherical particles (Fig. 1; Supplementary Table S2). The number-average molecular weights of pristine MPs ranged from 2.28×10^4 to 7.84×10^4 Da (Supplementary Table S2). Among the MPs, PVC possessed the highest specific surface area (SSA, 4.71 ± 0.05 1 $m^2\ g^{-1}$), whereas the SSA of other polymers did not exceed 1 $m^2\ g^{-1}$. The pristine MPs exhibited a hydrophobic surface, and their water contact angle followed the order PE > PP > PS ≈ PVC > PET (Fig. 1g). This trend is consistent with differences in polymer backbone chemistry, with nonpolar polyolefins (PE and PP) exhibiting the highest hydrophobicity, while the presence of ester functional groups in PET confers increased surface polarity and lower contact angles[35,36].

O_3- or UV-aging substantially modified the physicochemical characteristics of all MPs, as evidenced by morphological, structural, and surface-chemical changes (Fig. 1; Supplementary Table S2). SEM images showed that O_3 or UV exposure caused clear surface

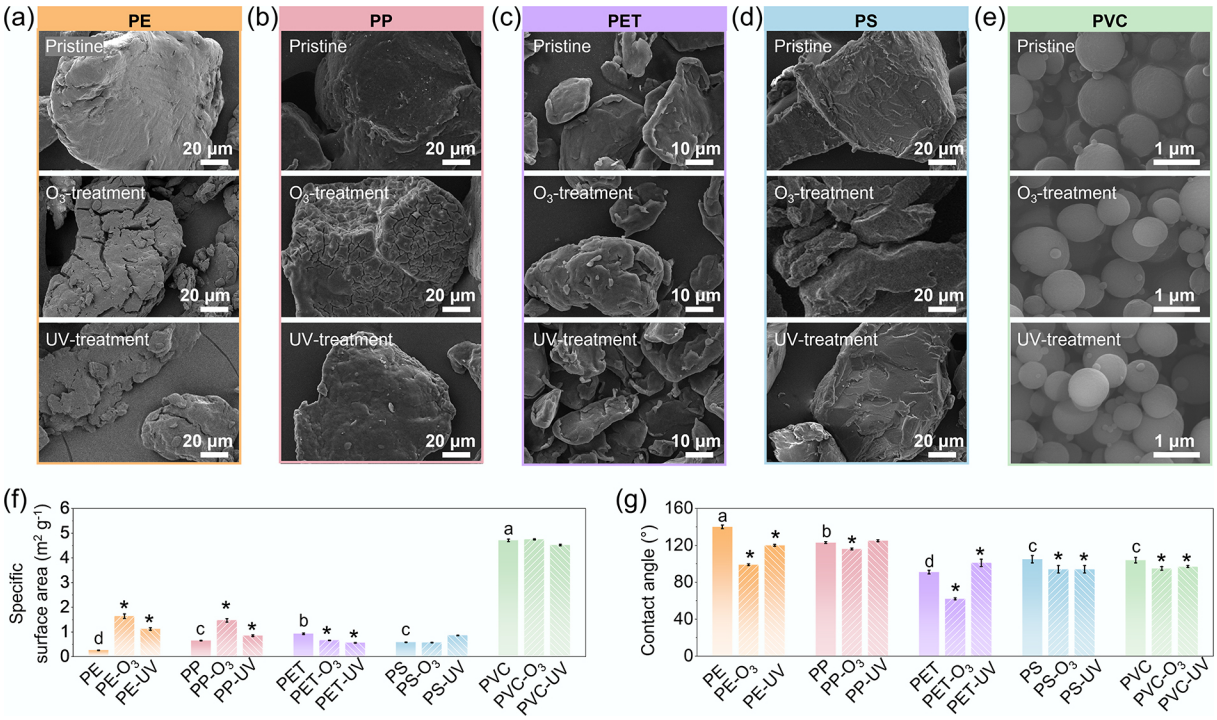

Fig. 1 Physicochemical properties of pristine, O_3-aged, and UV-aged MPs. (**a**)–(**e**) Scanning electron microscopy (SEM) images, (**f**) specific surface area (SSA), and (**g**) water contact angle for pristine and aged MPs. Suffixes '-O_3' and '-UV' denote ozone- and UV-aged samples, respectively. Error bars indicate ±1 standard deviation from triplicate measurements. In panels (**f**) and (**g**), lowercase letters indicate significant differences among pristine MPs (one-way ANOVA, $p < 0.05$), whereas asterisks denote significant differences between aged samples and their pristine counterparts (two-sample t-test, $p < 0.05$).

weathering features on MPs, including cracks, pits, and rough textures. These alterations were especially pronounced for PE and PP (Fig. 1a, b), where aged samples showed extensive surface fissures, cross-cracking, and fragmentation. In contrast, the morphology of PVC remained nearly unchanged (Fig. 1e), which is consistent with its relatively rigid and glassy polymer matrix[37]. Quantitative analyses confirmed significant SSA increases after both O_3 and UV aging (Fig. 1f), especially for PE and PP, which rose by 70%–160% ($p < 0.05$). PET and PS exhibited smaller increases, indicating moderate oxidation. The increased SSA and micropore volume among aged MPs (Supplementary Table S2) suggest that oxidative and photo-degradative processes led to polymer chain breakage or cross-linking[38,39], with the extent of these changes depending strongly on polymer types.

Oxidative and photochemical aging also modified the surface functionalities of MPs. XPS results revealed elevated O/C ratios and higher percentages of hydrophilic carbon species following aging (Supplementary Fig. S3; Supplementary Table S2). These changes are commonly attributed to oxidation-induced formation of oxygen-containing surface functional groups[24], including carbonyl (C=O) and hydroxyl (–OH) moieties, as evidenced by XPS and FTIR (Supplementary Figs S3, S4). Consequently, the relative abundance of hydrophobic carbon decreased, in line with the reduced contact angles observed for most polymers. For instance, the contact angle of PE decreased from 129° ± 4° to 91° ± 6° (O_3-aged) and 84° ± 5° (UV-aged) (Fig. 1g). Overall, O_3- and UV-induced aging increased the surface roughness, oxygen content, and hydrophilicity of MPs, with the magnitude of change depending on polymer chemistries. Flexible polyolefins (PE and PP) were more vulnerable to oxidation than rigid aromatic polymers (PS and PET).

Overall distribution coefficients for DOM adsorption depends on polymer type

The overall adsorption affinity of DOM on MPs reflected the combined result of polymer types, aging treatments, and DOM compositions (Fig. 2). For all five types of MPs, the isotherm data was well fitted by the Freundlich model, with coefficients of determination (R^2) ranging from 0.806 to 0.995 (Supplementary Table S3), indicating adsorption occurring on heterogeneous surfaces with non-uniform energy distributions. The relative adsorption affinities of SRFA and SRHA onto different MPs were compared based on the apparent distribution coefficient (K_d). In general, for SRFA, K_d values did not exhibit a significant difference among the polymer types (Fig. 2a), whereas for SRHA, K_d values varied largely among different polymer types, with the lowest K_d value for PP (Fig. 2b). Besides, for pristine aromatic polymers (PS, PET) and the polar PVC, SRHA exhibited higher K_d values (0.15–0.3) than SRFA (around 0.13) (Fig. 2). This difference is consistent with the higher aromaticity of SRHA[40], which can enhance π–π stacking interactions with the aromatic backbones of PS and PET (Supplementary Table S4)[15,41]. For PET specifically, ester (carbonyl/ether) groups provide polar sites that can form hydrogen bonds with oxygen-containing functionalities in both SRHA and SRFA, thereby contributing to the PET–DOM association. However, hydrogen bonding alone is unlikely to explain the higher K_d values observed for SRHA relative to SRFA, because SRFA often contains a higher density of oxygenated acidic functional groups (e.g., carboxyl groups) than SRHA[27]. For PVC, the preferential adsorption of SRHA relative to SRFA is likely governed by hydrophobic interactions, with additional contributions from hydrogen bonding and interactions involving C–Cl moieties that have been proposed to contribute to SRHA retention on PVC surfaces[14].

Aging treatments significantly altered DOM adsorption behavior on MPs, with effects that depended on both polymer type and DOM

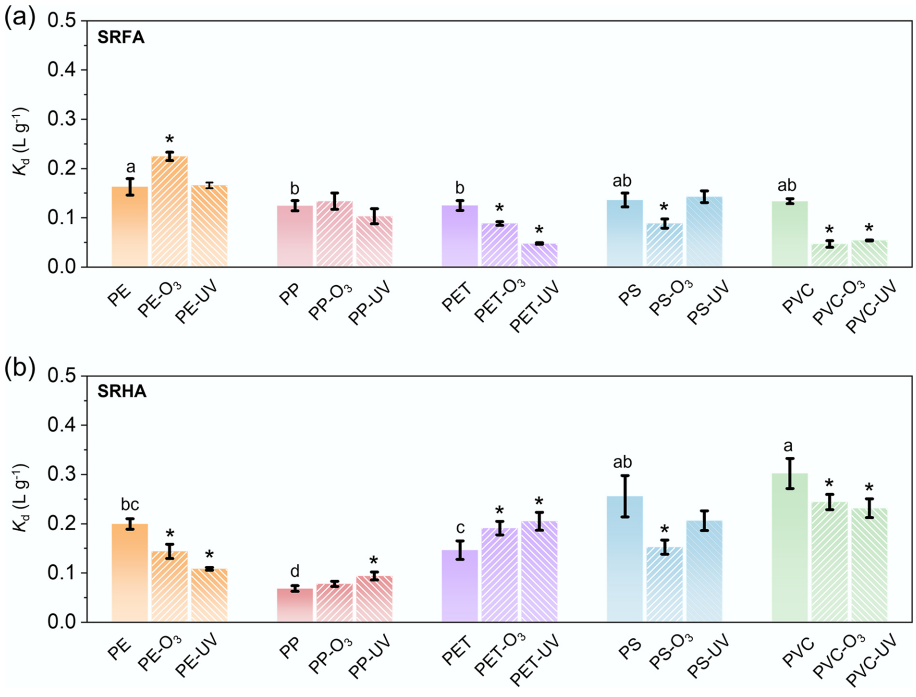

Fig. 2 Distribution coefficient (K_d) of (**a**) SRFA, and (**b**) SRHA obtained from the sorption experiments. Error bars indicate ±1 standard deviation from three replicate measurements. Suffixes '-O_3' and '-UV' denote ozone- and UV-aged MPs, respectively. Lowercase letters denote significant differences among pristine MPs (one-way ANOVA, $p < 0.05$). Significant differences between aged and corresponding pristine samples are denoted by asterisks (two-sample t-test, $p < 0.05$).

https://doi.org/10.48130/ebp-0026-0004

composition. For SRFA, K_d decreased significantly after aging on PVC (65.0% for O_3-aging; 59.6% for UV-aging) and PET (29.3% for O_3-aging; 61.8% for UV-aging), whereas PS showed a large decrease under O_3-aging (35.2%), but only a minor change under UV-aging (Fig. 2a; Supplementary Fig. S5). The reduced SRFA adsorption on aged PET, PS, and PVC is consistent with oxidation-induced surface oxygenation, reflected by higher O/C ratios or increased hydrophilic carbon fractions (Supplementary Table S2), as well as enhanced surface hydrophilicity indicated by reduced contact angles (Fig. 1g). Together, these changes can weaken hydrophobic and π–π interactions between MPs and SRFA[15,24]. In contrast, O_3-aging increased K_d on PE by 38.0% relative to pristine PE, consistent with the introduction of oxygen-containing functional groups that create new polar interaction sites, including potential hydrogen bonding, with oxygenated moieties in SRFA[16,25]. For SRHA, K_d decreased significantly after aging on PVC (19.2% for O_3-aging; 23.4% for UV-aging) and on PS (40.4% for O_3-aging; 19.4% for UV-aging) relative to the corresponding pristine MPs, (Fig. 2a; Supplementary Fig. S5), consistent with the trends observed for SRFA. In contrast to SRFA, however, K_d on PE decreased significantly after both O_3-aging (27.9%) and UV-aging (45.7%) relative to pristine PE, indicating that oxidative aging suppressed SRHA adsorption on PE. These results highlight that aging effects on DOM adsorption are polymer- and DOM-specific rather than universal.

Fluorescent components and molecular-weight fractions of adsorbed DOM vary across polymer type

To further elucidate how the polymer matrix and aging-induced physicochemical modification of MPs affect DOM adsorption, we analyzed the fluorescent components and molecular-weight fractions of adsorbed DOM (Figs 3, 4). EEM-PARAFAC resolved three main components for both SRFA and SRHA. The C1 component (Ex/Em = 270(334)/464 nm) represents aromatic- or quinone-like substances with high hydrophobicity and large molecular weight[42]. The C2 component (254/412 nm) corresponds to oxidized anthraquinone-like materials formed through microbial processing, and is moderately hydrophobic[43]. The C3 component (230/428 nm) is commonly associated with low molecular-weight and relatively hydrophilic compounds[33]. The overall hydrophobicity follows the order C1 > C2 > C3[44].

Because oxidative aging simultaneously alters MP physical structure (e.g., SSA/microporosity) and surface chemistry (e.g., hydrophilicity), the net changes in C1–C3 enrichment and MW selectivity are not necessarily monotonic but depend on polymer types and the aging pathways (O_3 vs UV). For SRFA (Fig. 3a), both O_3- and UV-aged PE exhibited increased intensities for all three PARAFAC components (C1–C3), indicating enhanced overall adsorption of

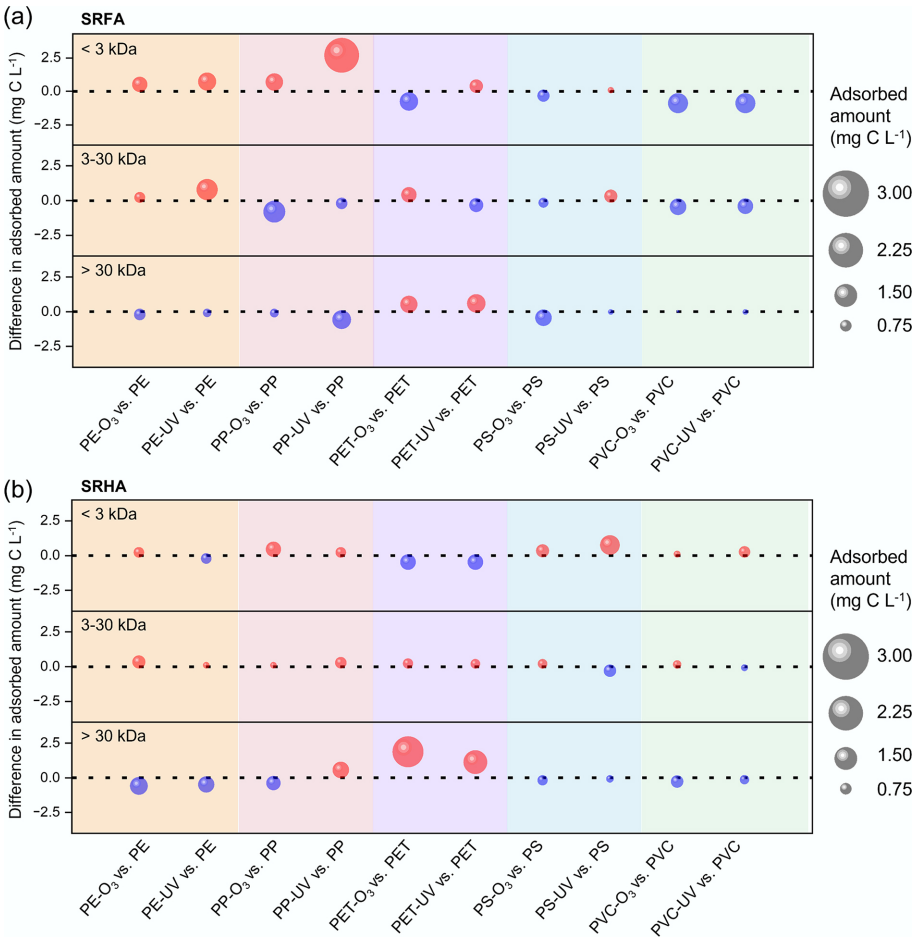

Fig. 3 Aging-induced changes in fluorescent components of (**a**) SRFA, and (**b**) SRHA adsorbed on MPs. Differences in PARAFAC component intensities between aged and pristine MPs are shown for each polymer and aging mode. Red markers indicate positive changes (greater adsorption after aging); blue markers indicate negative changes. Marker size is proportional to the absolute change in PARAFAC component intensity between aged and pristine MPs. Suffixes '-O_3' and '-UV' denote ozone- and UV-aged MPs, respectively.

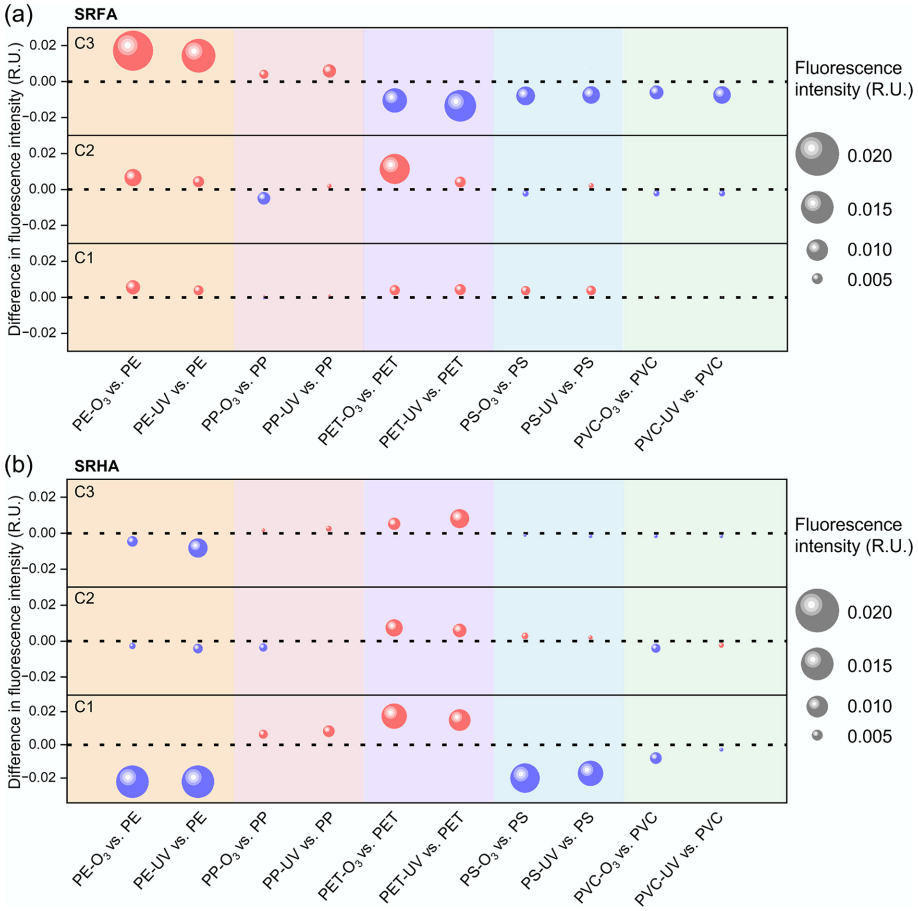

Fig. 4 Aging-induced changes in molecular-weight components of (**a**) SRFA, and (**b**) SRHA adsorbed on MPs. Differences in the adsorbed amounts of each molecular-weight fraction (< 3, 3–30, and > 30 kDa) between aged and pristine MPs are shown. Red markers indicate increased adsorption after aging, while blue markers indicate decreased adsorption. Marker size is proportional to the absolute change in adsorbed amount of each molecular-weight fraction between aged and pristine MPs. Suffixes '-O_3' and '-UV' denote ozone- and UV-aged MPs, respectively.

fluorescent SRFA fractions after aging, with O_3-aging showing a greater increase overall than UV-aging. In contrast, both O_3- and UV-aged PVC showed decreases in the intensities of all three components, with both aging pathways inducing a similar magnitude of reduction, consistent with the reduced adsorption reflected by the corresponding K_d values in Fig. 2a. Aging induced more heterogeneous and component-specific responses for PP and PS, with the direction and magnitude of changes depending on both polymer chemistry and aging pathway. In particular, O_3- and UV-aged PET exhibited pronounced decreases in the C3 component, despite concurrent increases in the C1 and C2 components, suggesting that the overall reduction in SRFA adsorption on aged PET (as reflected by K_d in Fig. 2a) was primarily driven by diminished association of the more hydrophilic C3 fraction. Notably, oxidative aging generally promoted enrichment of the more hydrophilic C3 component on polyolefins (PE and PP), while suppressing C3 enrichment on aromatic polymers (PET and PS) and on polar PVC, with UV-aging showing a greater decrease than O_3-aging for PET and PVC. These contrasting C3 trends are consistent with oxidation-induced increases in surface hydrophilicity (Supplementary Table S2; Fig. 1g), which may favor interactions with relatively hydrophilic, low-aromatic SRFA fractions on polyolefins while weakening hydrophobic interactions on aromatic or polar polymers. In addition, the development of microporosity on aged polyolefins (Supplementary Table S2; Fig. 1a, b) suggests that size-selective accessibility (size exclusion) may also contribute, as newly formed micro-/nano-pores can create internal sorption domains that are preferentially accessible to C3-associated relatively small DOM moieties[45,46].

For SRHA, the effects of aging on the enrichment of components (C1–C3) were likewise polymer-dependent and component-specific (Fig. 3b), but the overall response patterns differed from those observed for SRFA. Both O_3- and UV-aged PE showed decreases in the intensities of all three components (C1–C3), with the most pronounced decline observed for the aromatic, hydrophobic C1 component. Both aging pathways exhibited a similar magnitude of decrease in the C1 component for PE. Similarly, oxidative aging led to reduced enrichment of all three components on PVC. These decreases in C1–C3 enrichment on PE and PVC are consistent with the corresponding reductions in K_d values for SRHA (Fig. 2b). In contrast, both O_3- and UV-aged PET exhibited increases in all three components (C1–C3), with the strongest enhancement observed for the aromatic, hydrophobic C1 fraction, consistent with the overall increase in SRHA adsorption on aged PET as reflected by K_d (Fig. 2b); O_3-aging induced a slightly greater increase in the C1 component than UV-aging for PET. For PS, O_3- and UV-aged samples showed pronounced decreases in the C1 component despite concurrent increases in the C2 and C3 components, suggesting that the overall reduction in SRHA adsorption on aged PS (Fig. 2b) was primarily

https://doi.org/10.48130/ebp-0026-0004

driven by diminished association of the more hydrophobic C1 fraction; O_3-aging induced a slightly greater decrease in the C1 component than UV-aging for PS. Aging induced heterogeneous and component-specific responses for PP, with both the direction and magnitude of changes depending on polymer chemistry and aging pathway.

The molecular-weight distribution of adsorbed DOM further supports that aging modified sorption selectivity in a polymer-specific manner (Fig. 4). For SRFA (Fig. 4a), both O_3- and UV-aging enhanced the adsorption of low-molecular-weight fractions (< 3 kDa) on polyolefins (PE and PP), but reduced or only slightly affected the adsorption of higher-molecular-weight range fractions. This enrichment of low-molecular-weight fractions (< 3 kDa) is consistent with the increased hydrophilicity and microporosity (introducing size-selective pore accessibility) of aged PE and PP (Fig. 1a, b, g; Supplementary Table S2). Particularly, UV-aging induced a greater increase in low-molecular-weight fractions (< 3 kDa) than O_3-aging for PP. In contrast, oxidatively aged PET displayed enrichment of > 30 kDa fractions and heterogenous responses for low molecular fractions (< 3 and 3–30 kDa). Similarly, for PS, oxidative aging induced heterogeneous and fraction-specific responses in amount changes. Both O_3- and UV-aged PVC exhibited reduced adsorption of all three molecular weight fractions, (especially for the < 3 kDa fraction), which is consistent with changes in K_d (Fig. 2a), and in fluorescent components (Fig. 3a).

For SRHA, molecular-weight fractionation revealed polymer-dependent aging effects on DOM enrichment (Fig. 4b), with response patterns distinct from those observed for SRFA (Fig. 4b). Notably, both O_3- and UV-aged PET exhibited pronounced enrichment of the higher-molecular-weight fractions (3–30 and 30 kDa), which likely contributed to the increased K_d values observed for SRHA on aged PET (Fig. 2b). Particularly, O_3-aging induced a greater increase in the higher-molecular-weight fractions (> 30 kDa) than UV-aging for PET. In contrast, for PE, PS, and PVC, both O_3- and UV-aging led to a clear reduction in the enrichment of the > 30 kDa fraction, accompanied by heterogeneous and fraction-dependent changes in the lower-molecular-weight ranges (< 3 and 3–30 kDa). These trends suggest that the overall decrease in SRHA adsorption on aged PE, PS, and PVC (Fig. 2b) was primarily driven by diminished retention of high-molecular-weight SRHA components (> 30 kDa). Collectively, these results indicate that oxidative aging alters not only the extent but also the molecular-weight selectivity of SRHA adsorption on MPs in a polymer-specific manner.

Surface area and hydrophobicity govern DOM adsorption on MPs

To quantify the relative importance of MP physicochemical properties in DOM adsorption, we computed permutation feature importance using a trained random forest model, an established approach for evaluating the contributions of multiple input variables in complex environmental systems[34]. The results showed that, for SRFA, specific surface area (SSA) was the dominant predictor (65.2%), followed by hydrophilic carbon (15.3%), average particle size (9.7%), and micropore volume (5.2%), whereas hydrophobic carbon contributed less (4.6%) (Fig. 5a). This pattern highlights that SRFA adsorption is primarily governed by accessible sorption capacity (SSA/porosity) and surface polarity that can promote polar interactions (e.g., hydrogen bonding) with oxygen-containing functionalities in SRFA (Supplementary Table S4). For SRHA, the controlling factors were more distributed, with SSA (30.5%) and hydrophobic carbon (27.1%) as the two largest contributors, followed by micropore volume (18.2%), hydrophilic carbon (15.9%), and average particle size (8.2%) (Fig. 5b). The important role of hydrophobic carbon is consistent with a stronger role of hydrophobic and π–π-associated interactions for the more aromatic SRHA.

Collectively, these results indicate that oxidative aging modifies DOM adsorption on MPs through two competing effects: (1) oxidation-induced surface roughening and increased porosity enhance the number of physical sorption sites, while (2) increased surface oxygenation reduces hydrophobicity and weakens nonpolar interaction pathways. The net impact of aging on DOM adsorption therefore reflects the balance between these opposing mechanisms and depends on both polymer chemistry and DOM composition.

Conclusions

This study shows that DOM fractionation on microplastics is shaped by the coupled influences of polymer type, environmental aging, and DOM characteristics, rather than by any single controlling factor. (1) For polyolefins (PE and PP), oxidative aging promoted association with low-molecular-weight and hydrophilic SRFA fractions, consistent with increased surface oxidation and porosity. In contrast, for aromatic polymers (PET), aging enhanced pathways favoring enrichment of larger, more aromatic SRHA components. (2) Environmental aging further modified DOM adsorption in a polymer- and DOM-dependent manner, producing divergent effects on both adsorption capacity and fractionation. Aging pathways (O_3 vs UV) did not show a monotonic effect on DOM fractionation, with O_3-aging inducing a greater increase

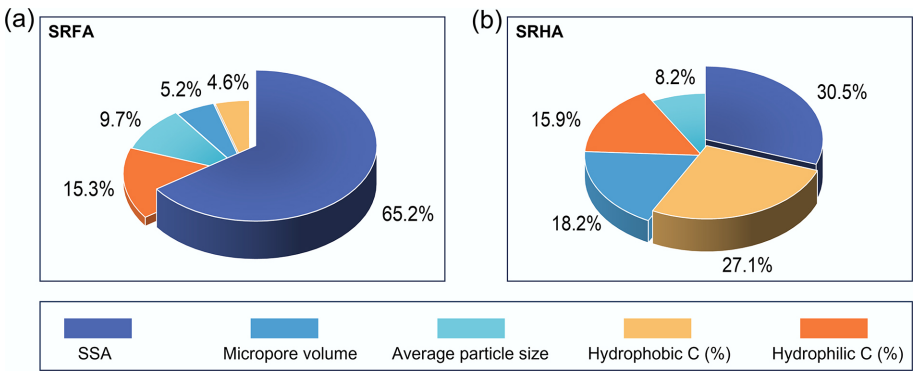

Fig. 5 Factors controlling the distribution coefficient (K_d) of (**a**) SRFA, and (**b**) SRHA on pristine and aged MPs. Pie charts show the contribution of each physicochemical property of pristine and aged MPs to the distribution coefficient derived from a neural-network model. Factors contributing less than 3% were omitted for clarity.

in the C1 component for PET, and a greater decrease in the C1 component for PS. (3) Regarding DOM characteristics, adsorption of SRFA showed similar K_d values across pristine polymers, while adsorption of SRHA varied significantly by polymer type, highlighting the role of DOM composition in mediating polymer-specific interactions. In addition, machine-learning analysis identified specific surface area (SSA) and surface carbon speciation as the dominant factors explaining variation in DOM distribution coefficients, with SSA accounting for 65.2% and 30.5% of the variance for SRFA and SRHA, respectively. These results emphasize that DOM adsorption behavior is influenced by both physical sorption capacity and interfacial chemistry.

Taken together, these findings demonstrate that DOM–microplastic interactions cannot be generalized across polymers or aging states. Instead, DOM fractionation reflects polymer-specific surface properties that evolve during environmental weathering. By linking measurable surface descriptors to DOM adsorption and selectivity, this work provides a mechanistic basis for incorporating DOM effects into predictions of microplastic transport, transformation, and contaminant interactions in natural aquatic systems. In particular, the quantity and composition of DOM adsorbed onto different types of microplastics can be used to assess the colloidal stability and mobility of MPs in aqueous environments. Moreover, the adsorbed ecological corona influences the interactions between microplastics and coexisting contaminants, affecting their bioavailability and fate in the environment.

Supplementary information

It accompanies this paper at https://doi.org/ebp-0026-0004.

Author contributions

The authors confirm their contributions to the paper as follows: Xiaoxia Zhang: writing – review and editing, investigation, methodology, formal analysis; Yan Lin: methodology, formal analysis; Mengting Zhao: investigation, methodology, formal analysis; Meiling Zhu: investigation, methodology, formal analysis; Tianchi Cao: writing – original draft, writing – review & editing, methodology, visualization, formal analysis; Thilo Hofmann: writing – review and editing, methodology, formal analysis, funding acquisition; Wei Chen: writing – review and editing, conceptualization, supervision, resources, funding acquisition. All authors reviewed the results and approved the final version of the manuscript.

Data availability

The datasets used or analyzed during the current study are available from the corresponding author upon reasonable requests.

Funding

This work was supported by the National Natural Science Foundation of China (Grant Nos 22241602 and 22020102004) and Tianjin Municipal Science and Technology Bureau (Grant Nos 23JCYBJC01650 and 23JCQNJC01340). This work was also supported by the Austrian Science Fund, Cluster of Excellence COE7 (Grant DOI 10.55776/COE7 [Thilo Hofmann]).

Declarations

Competing interests

The authors declare that they have no conflict of interest.

Author details

[1]College of Environmental Science and Engineering, Ministry of Education Key Laboratory of Pollution Processes and Environmental Criteria, Tianjin Key Laboratory of Environmental Remediation and Pollution Control, Nankai University, 38 Tongyan Road, Tianjin 300350, China; [2]Sinopec Engineering Incorporation, Beijing 100101, China; [3]Department of Environmental Protection, Changchun Gold Research Institute Co., Ltd., Changchun 130000, China; [4]Department of Environmental Geosciences, Centre for Microbiology and Environmental Systems Science, University of Vienna, 1090 Vienna, Austria

References

[1] Alva PP, Thomas TA. 2025. Microplastics: a global threat to life and living. *Environmental Monitoring and Assessment* 197:725

[2] Li J, Zhao Y. 2025. Bioeffects of nanoplastics: DNA damage and mechanism. *Nano Letters* 25:1660−1665

[3] Du H, Peng C, Li Y, Shi X, Liu C, et al. 2025. Absorption of microplastics by terrestrial plants and their ecological risk. *New Contaminants* 1:e003

[4] Zhao B, Richardson RE, You F. 2024. Microplastics monitoring in freshwater systems: a review of global efforts, knowledge gaps, and research priorities. *Journal of Hazardous Materials* 477:135329

[5] Feng F, Ye W, Xiang S, Fan X, Liu X, et al. 2025. Factors influencing the migration and distribution of microplastics in the environment. *Frontiers of Environmental Science & Engineering* 19:142

[6] Chouchene K, da Costa JP, Chamkha M, Ksibi M, Sayadi S. 2023. Effects of microplastics' physical and chemical properties on aquatic organisms: state-of-the-art and future research trends. *TrAC Trends in Analytical Chemistry* 166:117192

[7] Pal D, Prabhakar R, Barua VB, Zekker I, Burlakovs J, et al. 2025. Microplastics in aquatic systems: a comprehensive review of its distribution, environmental interactions, and health risks. *Environmental Science and Pollution Research* 32:56−88

[8] Sun Y, Zhang Q, Deng Q, Bai N, Chen H. 2026. The damaging effects of polyethylene microplastics exposure on juvenile carp and the ameliorative role of *Opuntia Milpa alta* extract. *ENGINEERING Environment* 20:7

[9] Koelmans AA, Bakir A, Burton GA, Janssen CR. 2016. Microplastic as a vector for chemicals in the aquatic environment: critical review and model-supported reinterpretation of empirical studies. *Environmental Science & Technology* 50:3315−3326

[10] Sun Y, Ji J, Tao J, Yang Y, Wu D, et al. 2023. Current advances in interactions between microplastics and dissolved organic matters in aquatic and terrestrial ecosystems. *TrAC Trends in Analytical Chemistry* 158:116882

[11] Tan MM, Feng LJ, Bian SZ, Duan JL, Li XH, et al. 2024. Interaction of dissolved organic matters and microplastics regulates the transport of microplastics in saturated porous media. *ACS ES&T Engineering* 4:1230−1239

[12] Müller ND, Kirtane A, Schefer RB, Mitrano DM. 2024. eDNA adsorption onto microplastics: impacts of water chemistry and polymer physiochemical properties. *Environmental Science & Technology* 58:7588−7599

[13] He L, Zhuang WE, Hur J, Yang L. 2026. Interactions of microplastics, dissolved organic matter, and coexisting pollutants: mechanisms, environmental implications, and knowledge gaps. *Environmental Research* 289:123418

[14] Zhang J, Zhan S, Zhong LB, Wang X, Qiu Z, et al. 2023. Adsorption of typical natural organic matter on microplastics in aqueous solution: kinetics, isotherm, influence factors and mechanism. *Journal of Hazardous Materials* 443:130130

[15] Abdurahman A, Cui K, Wu J, Li S, Gao R, et al. 2020. Adsorption of dissolved organic matter (DOM) on polystyrene microplastics in aquatic environments: kinetic, isotherm and site energy distribution analysis. *Ecotoxicology and Environmental Safety* 198:110658

[16] Wang X, Wang X, Zhu W, Ding L, Liang X, et al. 2024. Insight into interactions between microplastics and fulvic acid: mechanisms affected by microplastics type. *Science of The Total Environment* 913:169427

[17] Schefer RB, Armanious A, Mitrano DM. 2023. Eco-corona formation on plastics: adsorption of dissolved organic matter to pristine and photochemically weathered polymer surfaces. *Environmental Science & Technology* 57:14707−14716
[18] Shahi NK, Kim JY, Dockko S. 2023. Process analysis of microplastic aging during the photochemical oxidation process and its effect on the adsorption behavior of dissolved organic matter. *Chemosphere* 341:139980
[19] Song Y, Zhao J, Zheng L, Zhu W, Xue X, et al. 2022. Adsorption behaviors and mechanisms of humic acid on virgin and aging microplastics. *Journal of Molecular Liquids* 363:119819
[20] Gao R, Cui K, Liang W, Wang H, Wei S, et al. 2022. Molecular weight-dependent adsorption heterogeneities of humic acid on microplastics in aquatic environments: further insights from fluorescence spectra combined with two-dimensional correlation spectroscopy and site energy distribution analysis. *Journal of Environmental Chemical Engineering* 10:108948
[21] Li J, Ma S, Li X, Wei W. 2022. Adsorption of tannic acid and macromolecular humic/fulvic acid onto polystyrene microplastics: a comparison study. *Water* 14:2201
[22] Yang H, Chen Z, Kong L, Xing H, Yang Q, et al. 2025. A review of eco-corona formation on micro/nanoplastics and its effects on stability, bioavailability, and toxicity. *Water* 17:1124
[23] Yousif E, Haddad R. 2013. Photodegradation and photostabilization of polymers, especially polystyrene: review. *SpringerPlus* 2:398
[24] Xu Y, Ou Q, van der Hoek JP, Liu G, Lompe KM. 2024. Photo-oxidation of micro- and nanoplastics: physical, chemical, and biological effects in environments. *Environmental Science & Technology* 58:991−1009
[25] Hu J, Lim FY, Hu J. 2023. Ozonation facilitates the aging and mineralization of polyethylene microplastics from water: behavior, mechanisms, and pathways. *Science of The Total Environment* 866:161290
[26] McColley CJ, Nason JA. 2024. Eco-corona formation on photooxidized plastics exposed to mixed organic matter. *Environmental Engineering Science* 41:448−458
[27] Ritchie JD, Perdue EM. 2003. Proton-binding study of standard and reference fulvic acids, humic acids, and natural organic matter. *Geochimica et Cosmochimica Acta* 67:85−96
[28] Sun Y, Yuan J, Zhou T, Zhao Y, Yu F, et al. 2020. Laboratory simulation of microplastics weathering and its adsorption behaviors in an aqueous environment: a systematic review. *Environmental Pollution* 265:114864
[29] Cao T, Zhao M, Zhang T, Chen W. 2025. Weathering pathways differentially affect colloidal stability of nanoplastics. *Environmental Science: Nano* 12:232−240
[30] Gewert B, Plassmann M, Sandblom O, MacLeod M. 2018. Identification of chain scission products released to water by plastic exposed to ultraviolet light. *Environmental Science & Technology Letters* 5:272−276
[31] Kowalczuk P, Durako MJ, Young H, Kahn AE, Cooper WJ, et al. 2009. Characterization of dissolved organic matter fluorescence in the South Atlantic Bight with use of PARAFAC model: interannual variability. *Marine Chemistry* 113:182−196
[32] Nguyen HV, Lee MH, Hur J, Schlautman MA. 2013. Variations in spectroscopic characteristics and disinfection byproduct formation potentials of dissolved organic matter for two contrasting storm events. *Journal of Hydrology* 481:132−142
[33] Stedmon CA, Bro R. 2008. Characterizing dissolved organic matter fluorescence with parallel factor analysis: a tutorial. *Limnology and Oceanography: Methods* 6:572−579
[34] Liu X, Gharasoo M, Shi Y, Sigmund G, Hüffer T, et al. 2020. Key physicochemical properties dictating gastrointestinal bioaccessibility of microplastics-associated organic xenobiotics: insights from a deep learning approach. *Environmental Science & Technology* 54:12051−12062
[35] Navaneetha Pandiyaraj K, Selvarajan V, Deshmukh RR, Gao C. 2008. Adhesive properties of polypropylene (PP) and polyethylene terephthalate (PET) film surfaces treated by DC glow discharge plasma. *Vacuum* 83:332−339
[36] Bîrleanu E, Mihăilă I, Topală I, Borcia C, Borcia G. 2023. Adhesion properties and stability of non-polar polymers treated by air atmospheric-pressure plasma. *Polymers* 15:2443
[37] Tomaszewska J, Sterzyński T, Woźniak-Braszak A, Banaszak M. 2021. Review of recent developments of glass transition in PVC nanocomposites. *Polymers* 13:4336
[38] Gradinaru LM, Vlad S, Spiridon I, Petrescu M. 2019. Durability of polyurethane membranes in artificial weathering environment. *Polymer Testing* 80:106144
[39] Pan Y, Yang M, Han S, Gao W, Dan Y. 2012. Study on the changing regularity of structure and properties of PC aged outdoor in western areas of China. *Journal of Applied Polymer Science* 125:2128−2136
[40] Thorn KA, Folan DW, MacCarthy P. 1989. Characterization of the International Humic Substances Society standard and reference fulvic and humic acids by solution state carbon-13 (13C) and hydrogen-1 (1H) nuclear magnetic resonance spectrometry. *Water-Resources Investigations Report 89-4196*. US Dept. of the Interior, US Geological Survey: Books and Open-File Reports. doi: 10.3133/wri894196
[41] Wu QY, Zhou TH, Du Y, Ye B, Wang WL, et al. 2020. Characterizing the molecular weight distribution of dissolved organic matter by measuring the contents of electron-donating moieties, UV absorbance, and fluorescence intensity. *Environment International* 137:105570
[42] Ding L, Luo Y, Yu X, Ouyang Z, Liu P, et al. 2022. Insight into interactions of polystyrene microplastics with different types and compositions of dissolved organic matter. *Science of The Total Environment* 824:153883
[43] Ishii SKL, Boyer TH. 2012. Behavior of reoccurring PARAFAC components in fluorescent dissolved organic matter in natural and engineered systems: a critical review. *Environmental Science & Technology* 46:2006−2017
[44] Truong HB, Huy BT, Ly QV, Lee YI, Hur J. 2019. Visible light-activated degradation of natural organic matter (NOM) using zinc-bismuth oxides-graphitic carbon nitride (ZBO-CN) photocatalyst: mechanistic insights from EEM-PARAFAC. *Chemosphere* 224:597−606
[45] Tan Y, Kilduff JE. 2007. Factors affecting selectivity during dissolved organic matter removal by anion-exchange resins. *Water Research* 41:4211−4221
[46] Hao L, Ma H, Xing B. 2024. Surface characteristics and adsorption properties of polypropylene microplastics by ultraviolet irradiation and natural aging. *Science of The Total Environment* 944:173962